Food & Function

ROYAL SOCIETY OF CHEMISTRY

PAPER

View Article Online
View Journal | View Issue



Cite this: *Food Funct.*, 2025, **16**, 539

# *Solanum lycopersicum* derived exosome-like nanovesicles alleviate restenosis after vascular injury through the Keap1/Nrf2 pathway†

Hechen Shen, ‡[a,b,c,d,e] Meng Zhang,‡[a,b,c,d,e] Dachang Liu,‡[b,c,d,e,g,h] Xiaoyu Liang,[b,c,d,e] Yun Chang,[b,c,d,e] Xiaomin Hu*[b,c,d,e,f,g,h] and Wenqing Gao*[b,c,d,e,f,g,h]

Received 20th August 2024,
Accepted 28th November 2024

DOI: 10.1039/d4fo03993a

rsc.li/food-function

Despite the significant alleviation of clinical cardiovascular diseases through appropriate interventional treatments, the recurrence of vascular restenosis necessitating reoperation remains a substantial challenge impacting patient prognosis. Plant-derived exosome-like nanovesicles (PELNs) are integral to interspecies cellular communication, with their functions and potential applications garnering significant attention from the research community. This study extracted *Solanum lycopersicum*-derived exosome-like nanovesicles (SL-ELNs) and demonstrated their inhibition of PDGF-BB-induced proliferation, migration, and phenotypic transformation of vascular smooth muscle cells (VSMCs). Mechanistically, miRNA164a/b-5p within the SL-ELNs reduced the expression of Keap1 mRNA, thereby increasing nuclear translocation of Nrf2 and enhancing the expression of antioxidant genes to alleviate oxidative stress. In a mouse carotid artery injury model, it was further confirmed that miRNA164a/b-5p within the SL-ELNs could inhibit neointimal hyperplasia. These results suggest that SL-ELNs inhibit VSMCs proliferation, migration, and phenotypic transformation, and they might be potential therapeutic agents for the prevention or treatment of restenosis.



## Introduction

Although appropriate interventional therapy significantly alleviates clinical cardiovascular disease, elevated restenosis and reintervention rates remain a significant limitation of revascularization procedures, particularly in patients with coronary artery disease.[1] Vascular smooth muscle cells (VSMCs) play a key role in the development of vascular restenosis.[2] Following vascular injury, cytokines such as platelet-derived growth factor BB (PDGF-BB) accumulate, transitioning VSMCs from a normal contractile state to a pathological synthetic state. This transformation can induce VSMCs to migrate toward the vascular intima and proliferate excessively, ultimately leading to severe intimal hyperplasia.[3] Despite efforts to prevent restenosis using systemic agents, the topical application of rapamycin and paclitaxel *via* drug-eluting stents remains the predominant approach. This approach is preferred primarily because of the significant adverse effects associated with systemic administration, including myelosuppression, paresthesias, gastrointestinal toxicity, and hepatic and renal impairment.[4–6] Therefore, there is considerable research interest in exploring safer natural products as alternative clinical agents for treating vascular restenosis.[7]

Similar to animal cells, plant cells also release nanoscale vesicles known as plant-derived exosome-like nanovesicles (PELNs).[8,9] These vesicles can potentially deliver bioactive compounds, including nucleic acids, to other species, thereby initiating therapeutic effects. For example, yam-derived exosome-like nanovesicles stimulate osteoclast formation, thereby preventing osteoporosis in mice.[10] Additionally, Liu *et al.* recently demonstrated that mtDNA from artemisia-derived exosome-like nanovesicles (ELNs) can remodel tumor-associated macrophages through the cGAS-STING pathway.[11]

[a]*The Third Central Clinical College of Tianjin Medical University, Tianjin 300170, China*
[b]*Department of Heart Center, The Third Central Hospital of Tianjin, 300170, China*
[c]*Tianjin Key Laboratory of Extracorporeal Life Support for Critical Diseases, Tianjin 300170, China*
[d]*Tianjin ECMO Treatment and Training Base, Tianjin 300170, China*
[e]*Artificial Cell Engineering Technology Research Center, Tianjin 300170, China*
[f]*Medical College, Tianjin University, Tianjin, 300072, China*
[g]*School of Medicine, Nankai University, Tianjin 300170, China*
[h]*Nankai University Affiliated Third Center Hospital, Nankai University, Tianjin 300170, China*

†Electronic supplementary information (ESI) available. See DOI: https://doi.org/10.1039/d4fo03993a

‡These authors have contributed equally to this work and share first authorship.

Unlike animal-derived exosomes, PELNs can be easily isolated and purified in large quantities. Therefore, they offer a sustainable and cost-effective therapeutic approach, overcoming the limitations of synthetic nanovesicles.

*Solanum lycopersicum* (SL) contains an elevated concentration of antioxidants, including lycopenes, carotenoids, vitamin C, glutathione, and phenolic acids,[12,13] which exhibit favorable effects on all-cause mortality and etiological-specific mortality.[14] Furthermore, epidemiological studies have highlighted the beneficial effects of *Solanum lycopersicum* and its derivatives on vascular function.[15,16] Previous research has demonstrated the potential importance of lycopene in inhibiting allograft atherosclerosis.[17] Based on this, ELNs present in *Solanum lycopersicum* may play a role in preventing vascular restenosis after injury. This study successfully extracted safe and absorbable *Solanum lycopersicum*-derived ELNs (SL-ELNs) and investigated their roles and molecular mechanisms in regulating proliferation, migration, and phenotypic transformation in VSMCs. These findings suggest that SL-ELNs could serve as potential bioactive substances for the prevention and treatment of vascular restenosis.

# Methods

### Cell and animal lines

VSMC, L929 and HEK293T cell lines were obtained from the American Type Culture Collection (ATCC) and subsequently verified. These cell lines were maintained in high-glucose Dulbecco's modified Eagle's medium (DMEM; Gibco, USA) or DMEM-F12 supplemented with 10% fetal bovine serum (FBS; AusgeneX, Australia) and 1% penicillin/streptomycin (Solarbio, China). The cells were cultured at 37 °C in a humidified atmosphere containing 5% $CO_2$ and 95% air.

Male C57BL/6J mice (6–8 weeks old) were procured from Beijing Vital River Laboratory Animal Technology Co., Ltd (Beijing, China). The mice were housed under specific pathogen-free (SPF) conditions at the Tianjin Third Central Hospital Animal Laboratory, with a 12 h light/dark cycle, a temperature of 20–25 °C, and 40–70% humidity. The experimental procedures were submitted for approval to the Experimental Animal Ethics Committee of Nankai University (approval number: 2022-SYDWLL-000483).

### Isolation and identification of SL-ELNs

100 g fresh *Solanum lycopersicum* was washed with purified water and blended at high speed for 5 min. The juice was centrifuged sequentially at 1000*g* for 10 min, 3000*g* for 30 min, and 10 000*g* for 30 min to remove large plant tissues and debris. The supernatant was subsequently ultracentrifuged at 150 000*g* for 1 h, and the microspheres were resuspended in 5 ml phosphate-buffered saline (PBS). For further purification, the suspension was layered onto sucrose gradients (8%, 30%, 45%, and 60%) and ultracentrifuged at 150 000*g* for 1 h. SL-ELN fractions were collected from three layers (8%/30%, 30%/45%, and 45%/60%) and stored at −80 °C.

The size distribution and zeta potential of the SL-ELNs were measured using ZetaView (version 8.05.14 SP7). Samples were stained with 1% (w/v) uranyl acetate and imaged using a transmission electron microscope (TEM; JEM-2100F, Tokyo, Japan).

### Carotid arterial restenosis model

The animal care and experimental protocols followed the National Institutes of Health Guide for the Care and Use of Laboratory Animals guidelines. The carotid arterial restenosis model was established as previously described.[18] Briefly, male mice (22–25 g) were anesthetized using an intraperitoneal injection of sodium pentobarbital (50 mg $kg^{-1}$). The right carotid artery was exposed, the proximal external carotid artery was ligated, and the internal and common carotid arteries were clamped. After making a transverse incision proximal to the ligation, a guide wire (0.38 mm diameter, C-SF-15-15; Cook, Bloomington, USA) was inserted through the incision into the left common carotid artery. After rotating and sliding the wire three times, it was removed, blood flow was restored, and the incision was sutured. Sham-operated mice underwent an identical procedure without arterial injury. Different dose groups (0 mg $kg^{-1}$, 0.5 mg $kg^{-1}$, 1 mg $kg^{-1}$ and 2 mg $kg^{-1}$) were established to determine the optimal dose of SL-ELNs on vascular restenosis. Following a 28 day treatment regimen, vascular samples were meticulously collected. At the end of the experiment, all mice were euthanized humanely using an overdose of anesthetic.

### Uptake of SL-ELNs

SL-ELNs were suspended in Dio solution (ThermoFisher, V22886) and incubated for 30 min. Subsequently, the samples were ultracentrifuged at 150 000*g* for 1 h to eliminate unbound dye. Following thorough washing and resuspension in PBS, the Dio-labeled SL-ELNs were prepared for experimental use.

For *in vitro* experiments, SL-ELNs were incubated with VSMCs under light-protected conditions and observed using a confocal laser scanning microscope (Olympus, FV3000, Japan). For *in vivo* studies, Dio-labeled SL-ELNs (25 mg $kg^{-1}$) were administered to mice *via* gavage. The fluorescence expression and distribution of SL-ELNs in tissues were evaluated using the Maestro™ system (CRi, Shawano, USA).

### CCK-8

Following treatment, VSMCs were incubated in a medium supplemented with 10% CCK-8 reagent (Eason, Shanghai, China) at 37 °C for 1 h. Cell viability was assessed by measuring the optical density (OD) value at 450 nm using a microplate reader (Victor Nivo™ FA1604S, USA).

### Cell proliferation

The proliferation of VSMCs was evaluated according to the instructions provided in the EdU-488 Cell Proliferation Kit (C0071S, Beyotime). EDU-positive cells were quantified and normalized to the total number of Hoechst 33342-stained cells. Furthermore, cell cycle analysis was conducted using a cell cycle assay kit (E-CK-A351, Elabscience). Data acquisition

 

and analysis were performed using FlowJo software (version 10.7.2).

### Cell migration

Cells were subjected to a wound healing assay by scratching the cell monolayer with a 200 μL pipette tip. After appropriate treatments, cell migration into the wound area was assessed. In addition, a transwell migration assay was conducted by seeding cells in the upper chamber, while 600 μL of DMEM supplemented with 20% FBS was added to the lower chamber. Following a 24 h incubation, cells were fixed with 4% formaldehyde and stained with crystal violet. Migratory cells were visualized using a Nikon Eclipse 80i microscope (Nikon, Chiyoda, Japan). The degree of wound closure and the number of migrated cells were quantified using ImageJ software (version 1.8.0.112).

### Oxidative stress

Oxidative stress was measured using a reactive oxygen species (ROS) assay kit (Beyotime, S0033S) according to the manufacturer's instructions. Mitochondrial membrane potential (MMP) disruption was assessed using a JC-1 Enhanced MMP Assay Kit (Beyotime, C2003S).

### Quantitative polymerase chain reaction (qPCR) analysis

Total RNA was collected using TRIzol (ThermoFisher Scientific) and reverse-transcribed. The amplified cDNA was synthesized using Revertra Ace and gDNA remover (Toyobo, Japan). qPCR was performed with GoTaq qPCR Master Mix (A6001, Promega, USA). The primer sequences used were listed in Table S4.†

### Small RNA-sequencing of SL-ELNs

RNA from SL-ELNs was isolated using TRIzol. Small RNA was extracted using PAGE electrophoresis for library preparation and sequencing. Small RNA-sequencing of SL-ELNs was performed using a BGISEQ-500 platform (BGI Group, Shenzhen, China). The sequence reads were mapped to known plant mature miRNAs from miRBase22.0, and mapping statistics were generated.

### Lentivirus and adeno-associated virus (AAV) transfection

Lentivirus and AAV vectors were purchased from GeneChem Co., Ltd (Shanghai, China). *In vitro*, VSMCs were cultured in six-well plates to a suitable density and transfected with Lentivirus-Keap1 at a multiplicity of infection of 50. Following transfection, the cells were selected with puromycin for one week. *In vivo*, gene overexpression in mice was induced using AAV serotype 9 (AAV9) vectors carrying Keap1 under the control of the SM22α promoter (AAV9-SM22α-MCS-3Flag-SV40-Keap1; vector number: GV597). AAV9-SM22α-MCS was used as the negative control. Mice were injected with either AAV9-NC or AAV9-Keap1 ($1.0 \times 10^{12}$ v.g.) in 200 μL of PBS *via* the tail vein.

### Dual-luciferase reporter assay

The wild-type (WT) and mutant 3′-UTR fragments of Keap1 were synthesized by GeneChem Co., Ltd and subsequently cloned into the GV272 reporter vector (SV40-firefly luciferase-MCS). miRNA164a/b-5p mimic and inhibitor synthesized by Sangon Biotech. The detailed sequences of the WT and mutant 3′-UTR fragments of Keap1 are provided in ESI 2.†

For the dual-luciferase reporter assay, HEK293T cells were co-transfected with either miRNA164a/b-5p mimic, GV272-Keap1-WT, or GV272-Keap1-Mut reporter plasmids, alongside the CV045 plasmid (TK promoter-Renilla luciferase). All plasmid transfections were performed using the Lipofectamine 2000 transfection reagent (Invitrogen, USA). Luciferase activity was quantified using the Dual-Glo™ Luciferase Assay System (E2920, Promega) according to the instructions provided by the manufacturer.

### Hematoxylin and eosin staining (HE staining)

Vascular tissues were collected, fixed in 4% paraformaldehyde, and embedded in paraffin. Tissue sections, 5 μm thick, were prepared and stained with HE following the instructions provided with the HE staining kit (Solarbio). Visualization was performed using a Nikon ECLIPSE E100 light microscope.

### Western blot (WB)

Protein extraction from VSMCs or vascular tissues was conducted using RIPA buffer (CW2334, CWBIO). Protein concentrations were determined using a BCA protein assay kit (CW0014S, CWBIO). Samples were denatured at 95 °C, mixed with SDS-PAGE loading buffer, and separated by SDS-PAGE. Proteins were transferred to PVDF membranes, blocked with 5% skim milk for 1 h, and incubated overnight at 4 °C with primary and secondary antibodies (1 : 5000, affinity, S0001/2). Detection was performed using enhanced chemiluminescence (ECL), and signals were analyzed using imaging software (Protein Simple, USA).

The primary antibodies used were α-SMA (1 : 20 000, Proteintech, 67735-1-Ig), OPN (1 : 1000, ABclonal, A1499), PCNA (1 : 1000, Cst, #13110), Cyclin D1 (1 : 200, Abcam, ab16663), MMP2 (1 : 1000, Proteintech, 66366-1-Ig), MMP9 (1 : 1000, Proteintech, 10375-2-AP), Keap1 (1 : 1000, Proteintech, 10503-2-AP), Nrf2 (1 : 5000, Proteintech, 16396-1-AP), HO-1(1 : 2000, Abcam, ab189491), Catalase (1 : 2000, Abcam, ab209211), NQO1 (1 : 10 000, Abcam, ab80588), Lamin B1 (1 : 5000, ABclonal, A11495), and GAPDH (1 : 50 000, ABclonal, A19056).

### Immunofluorescence

For immunofluorescence analysis, tissue sections or fixed cells (treated with 4% formaldehyde) were incubated overnight at 4 °C with the primary antibodies α-SMA (1 : 200), OPN (1 : 200), Keap1 (1 : 200), and Nrf2 (1 : 500). Subsequently, samples were incubated with conjugated secondary antibodies (1 : 200, Abcam). The nuclei were counterstained with diaminidine phenylindole (DAPI; Southern Biotech, USA). Fluorescence

images were captured using a confocal laser scanning microscope (Olympus, FV3000, Japan).

### Biocompatibility assay

Cell viability/cytotoxicity was measured using a Calcein/PI cell viability/cytotoxicity assay kit (Beyotime) according to the manufacturer's instructions. Subsequently, the concentration of alanine aminotransferase (ALT), aspartate aminotransferase (AST), blood urea nitrogen (BUN), and creatinine in mouse plasma was then determined by enzyme-linked immunosorbent assay (ELISA) kit (Elabscience).

### Statistical analysis

All data are expressed as the mean ± standard deviation. Statistical analysis and visualization were conducted using GraphPad software (version 8.0). Intergroup differences were evaluated *via* a one-way ANOVA, or Student's t-test, with statistical significance set at $P < 0.05$.

## Results

### Extraction and characterization of SL-ELNs

SL-ELNs were isolated and purified through sucrose gradient ultracentrifugation (Fig. 1A). The zeta potentials of SL-ELNs across different stratifications consistently ranged from −20 to −30 mV, with average sizes ranging from 120 to 140 nm (Fig. 1B and C). Notably, SL-ELNs at the 30/45% interface exhibited an elevated concentration ($2.2 \times 10^{10}$ particles per mL) (Table S1†). TEM (Fig. 1D) revealed that these SL-ELNs were classical circular vesicles characterized by lipid bilayers.

Moreover, Dio-labeled SL-ELNs were utilized to investigate uptake by VSMCs, revealing increased uptake at the 30/45% interface (Fig. 1E). Additionally, gavage administration in mice indicated that SL-ELNs were predominantly distributed in the abdomen, with fluorescence intensity decreasing over time (Fig. 1F). Consistently, SL-ELNs at the 30/45% interface exhibited a more pronounced distribution compared to other fractions across all time points. Finally, the composition of SL-ELNs was investigated. Using an equal mass (100 g) of *Solanum lycopersicum*, the protein and nucleic acid concentrations in SL-ELNs from the 30–45% fraction were found to be higher than those in the other groups (Fig. 1G). Based on these results, SL-ELNs from the 30–45% fraction were selected for subsequent experiments. Finally, the yield of SL-ELNs was 4.242 mg $kg^{-1}$ based on the protein concentration extracted from 100 g of *Solanum lycopersicum*, which is similar to the yield reported of other PELNs in the previous study.[19,20]

To evaluate the safety of SL-ELNs, mice received oral doses of 2 mg per kg per day for 14 consecutive days. Following administration, no significant changes in body weight or dietary intake were observed among the animals. Moreover, histological examination revealed no abnormalities in liver, kidney, spleen, heart, or lung tissues (Fig. S1A†). In addition, the organ coefficient was used as a key indicator of chronic toxicity in the *in vivo* experiments. The results showed no statistically significant differences between the two groups (Fig. S1B†). Furthermore, ELISA analysis indicated that SL-ELNs had no adverse effects on liver or kidney function in mice, as there were no significant differences in ALT, AST, BUN, or creatinine levels between the two groups (Fig. S1C†). In the *in vitro* experiments, Calcein AM/PI staining further confirmed that SL-ELNs did not significantly inhibit the viability of L929 cells (Fig. S1D†). In summary, our experiments successfully prepared SL-ELNs from *Solanum lycopersicum* and demonstrated their excellent biocompatibility.

### Impact of SL-ELNs on the phenotypic transition of VSMCs induced by PDGF-BB

Previous studies determined that treatment with 20 ng $mL^{-1}$ of PDGF-BB for 24 hours was optimal.[21,22] Increasing the concentration of SL-ELNs mitigated the reduction in cell viability induced by PDGF-BB. However, concentrations above 100 μg $mL^{-1}$ did not yield further significant improvements (Fig. S2†). Consequently, the concentration of 100 μg $mL^{-1}$ was selected for subsequent experiments.

As illustrated in Fig. 2A and B, immunofluorescence and WB revealed that PDGF-BB induced a phenotypic transition in VSMCs, as evidenced by the downregulation of the contractile phenotype-associated protein α-SMA, coupled with the upregulation of the synthetic phenotype-associated protein OPN. Notably, SL-ELN treatment effectively reversed these alterations.

Subsequently, VSMC proliferation and migration were further examined. As illustrated in Fig. 2C, SL-ELN treatment inhibited PDGF-BB-induced VSMC proliferation. Cell cycle analysis (Fig. 2D) showed that SL-ELN treatment prevented PDGF-BB-treated VSMCs from transitioning from the G0/G1 phase to the S phase. Wound healing (Fig. 2E) and transwell assays (Fig. 2F) demonstrated that SL-ELNs significantly inhibited the migration of PDGF-BB-induced VSMCs. Furthermore, the expression of proteins associated with proliferation and migration in VSMCs was analyzed (Fig. 2G). Compared to PDGF-BB induction alone, SL-ELN treatment reduced the expression of the cell cycle-related proteins PCNA and Cyclin D1, along with that of the migration-related proteins MMP2 and MMP9.

### Effect of SL-ELNs on carotid restenosis in mice

Additionally, the inhibitory effect of SL-ELNs on restenosis following vascular injury was evaluated using mouse carotid artery guidewire strain to simulate vascular injury. The optimal dose was determined to be 1 mg $kg^{-1}$, as the improvement in restenosis reached a plateau when the concentration of SL-ELNs exceeded 1 mg $kg^{-1}$ (Fig. S3†). The specific experimental process is shown in Fig. 3A. Histological examination revealed significant vascular stenosis in the injury group compared to the sham-operated group. However, treatment with SL-ELNs mitigated injury-induced carotid artery stenosis (Fig. 3B). Moreover, both the neointimal area and neointimal/media ratio were significantly reduced in the SL-ELNs group (Fig. 3C). Immunofluorescence and WB assays (Fig. 3D and E)

 

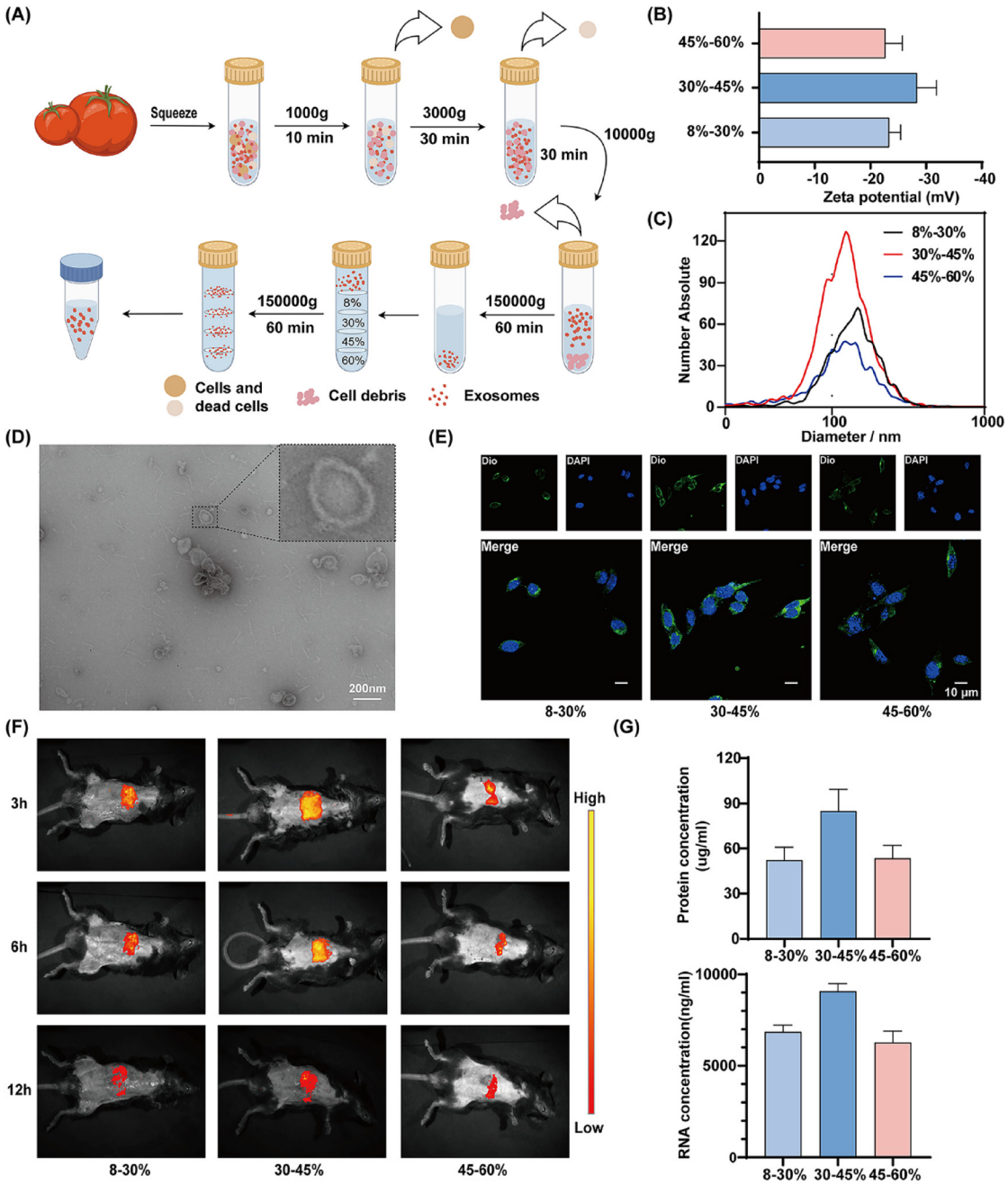


**Fig. 1** Characterization of *Solanum lycopersicum* derived exosome-like nanovesicles (SL-ELNs). (A) Flowchart of differential ultracentrifugation procedures for separation of LE-ELNs. (B) Zeta potential of the LE-ELNs ($n$ = 6). (C) Size distribution of the LE-ELNs. (D) TEM image of LE-ELNs. (E) Uptake of Dio-labeled LE-ELNs by VSMCs ($n$ = 3). (F) Uptake of Dio-labeled LE-ELNs by mice observed by intragastric administration ($n$ = 3). (G) Concentrations of protein and mRNA from within LE-ELNs ($n$ = 6).

further demonstrated that SL-ELNs attenuated the injury-induced phenotypic transformation of VSMCs.

### Mechanisms of SL-ELNs in regulating phenotypic transition

Oxidative stress is widely recognized as a significant contributor to vascular injury. The Keap1/Nrf2 signaling pathway is paramount in cellular defense mechanisms, playing an essential role in modulating the expression of critical antioxidant enzymes. In this pathway, Keap1 interacts with Nrf2, facilitating its ubiquitination and subsequent degradation. This interaction represents a pivotal regulatory step that modulates the activation of genes integral to antioxidant responses.

As shown in (Fig. S4†), SL-ELNs significantly alleviated oxidative stress-induced damage in VSMCs, including a reduction in ROS levels and an improvement in mitochondrial homeo-

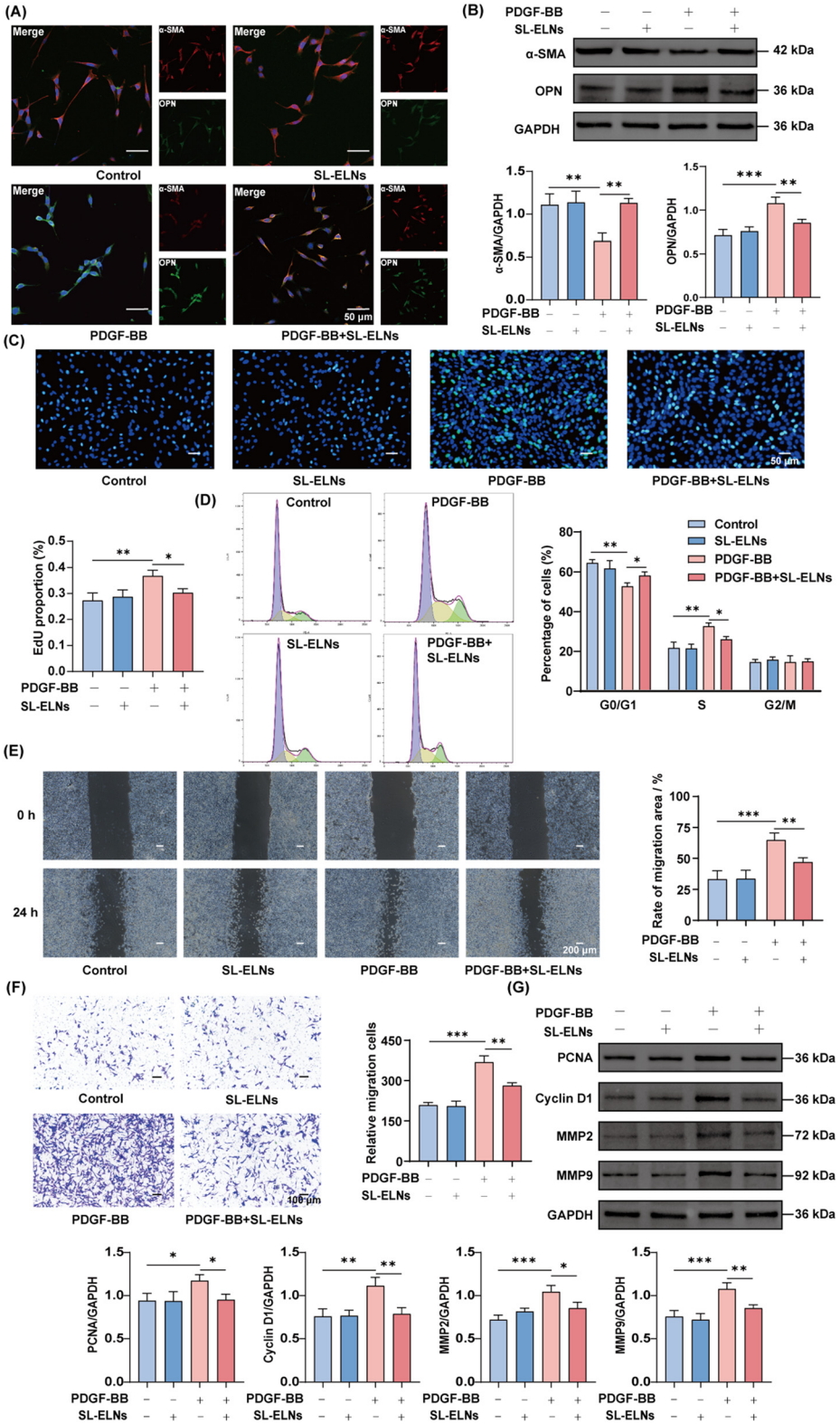


**Fig. 2** Influence of LE-ELNs on the phenotypic transition of VSMCs induced by PDGF-BB. (A) immunofluorescent staining of α-SMA and OPN in VSMCs. (B) Western blot and statistical analyses for protein level of α-SMA and OPN in VSMCs ($n$ = 3). (C) EDU staining and quantitative analysis of EDU positive cell ($n$ = 3). (D) Flow cytometric detection of cell cycle distribution and quantitative analysis of cell cycle distribution ($n$ = 3). (E) Wound healing assay and quantitative analysis of migration area ($n$ = 3). (F) Transwell assay and quantitative analysis of migratory cell ($n$ = 3). (G) western blot and statistical analyses for protein level of PCNA, cyclin D1, MMP2 and MMP9 in VSMCs ($n$ = 3). Data are expressed as mean ± SD (*$P$ < 0.05, **$P$ < 0.01 and ***$P$ < 0.005 were determined by one-way ANOVA and Tukey's *post hoc* test).

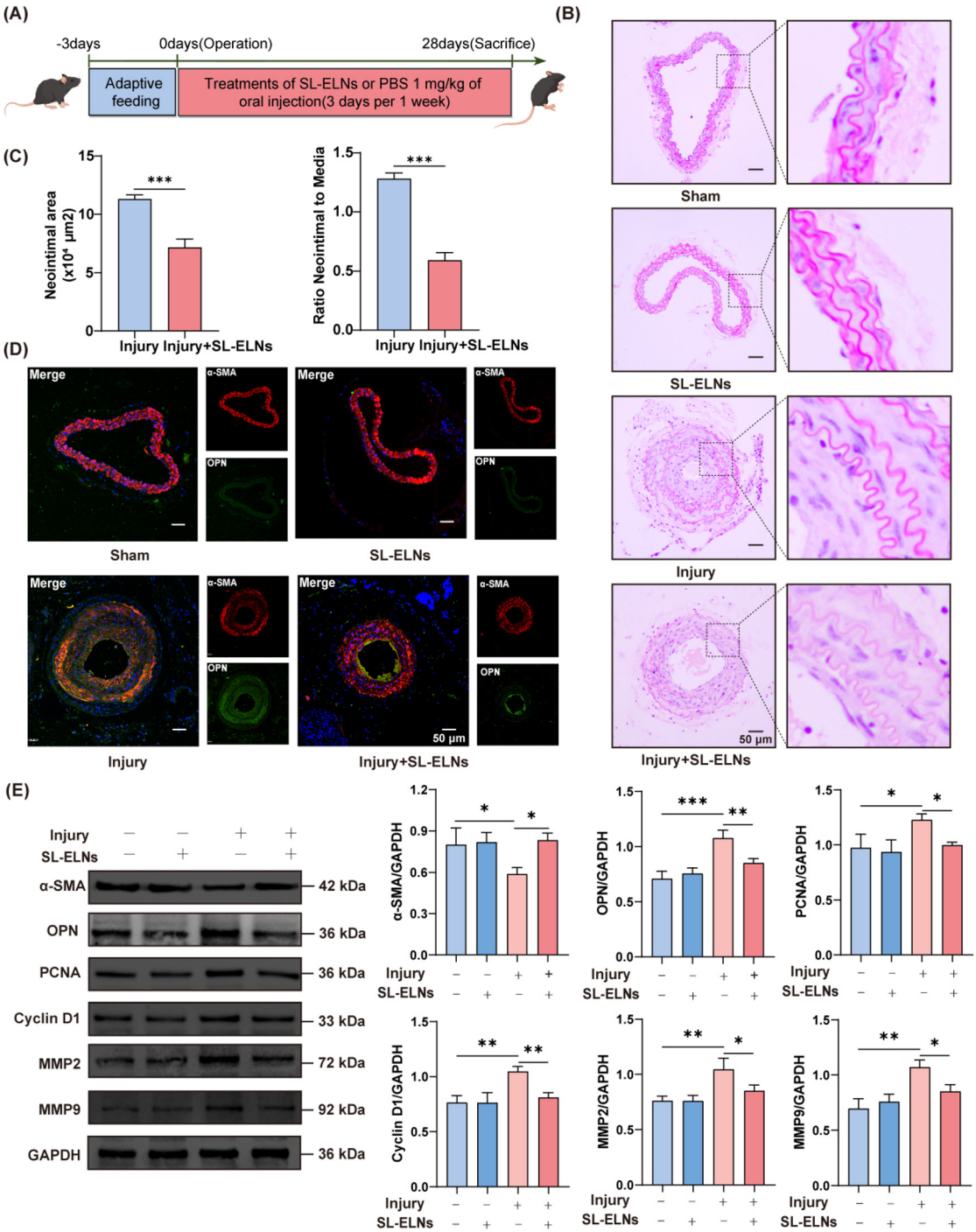


**Fig. 3** Influence of LE-ELNs on carotid restenosis in Mice. (A) Schematic diagram of the experimental procedure. (B) HE staining image of carotid arteries in mice ($n$ = 3). (C) Statistical analyses for the neointima area and the ratio of neointima area to the media area in mouse carotid artery ($n$ = 3). (D) Immunofluorescent staining of α-SMA and OPN in mouse carotid artery ($n$ = 3). (E) Western blot and statistical analyses for protein level of α-SMA, OPN, PCNA, cyclin D1, MMP2 and MMP9 in VSMCs ($n$ = 3). Data are expressed as mean ± SD (*$P$ < 0.05, **$P$ < 0.01 and ***$P$ < 0.005 were determined by one-way ANOVA and Tukey's *post hoc* test).

stasis. Additionally, the SL-ELNs group exhibited markedly lower Keap1 protein and mRNA expression levels compared to the PDGF-BB group (Fig. 4A and B). Immunofluorescence provided further evidence of the impact of SL-ELNs on Keap1 expression in injured vessels (Fig. 4C).

Exosomal miRNAs have been extensively studied for their significant role in cellular communication.[23] A detailed microarray analysis was performed to delineate the miRNA expression profile within SL-ELNs. As shown in Tables S2, S3† and Fig. 4D, 173 distinct miRNAs were identified, with the top

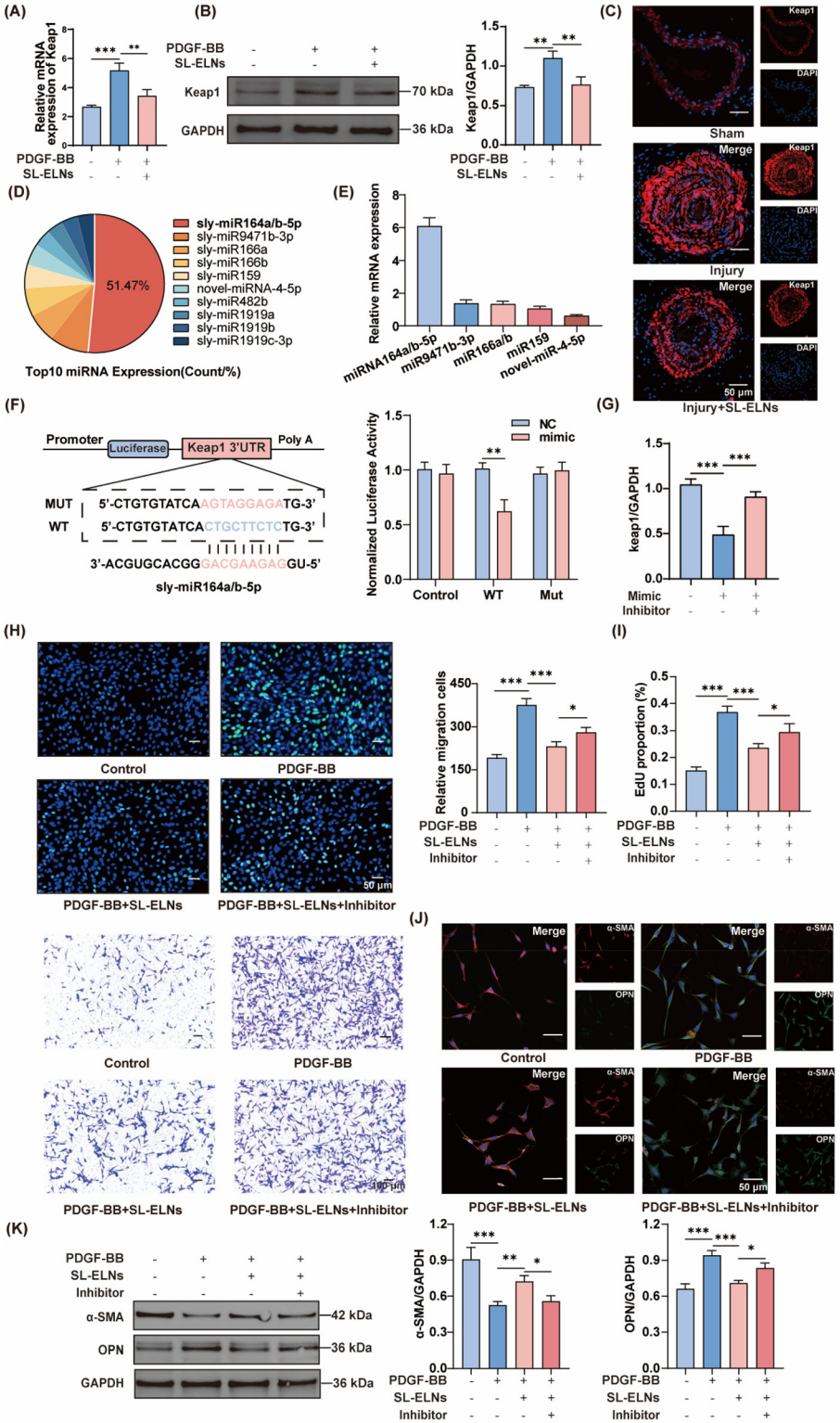


**Fig. 4** Mechanisms of SL-ELNs in regulating phenotypic transition. (A) qPCR analysis of Keap1 mRNA in VSMCs after exosomes were added ($n$ = 6). (B) Western blot and quantitative analysis of of Keap1 ($n$ = 3). (C) Immunofluorescent staining of Keap1 ($n$ = 3). (D) miRNA microarray results indicating relative percentage of miRNAs in Top10 miRNA reads. (E) qPCR analysis of top5 miRNA in VSMCs after exosomes were added ($n$ = 6). (F) Structure and luciferase result of dual luciferase reporter gene ($n$ = 3). (G) qPCR analysis of Keap1 in VSMCs after SL-ELNs and inhibitor were added ($n$ = 3). (H) EDU staining image of VSMCs and quantitative analysis of EDU positive cell ($n$ = 3). (I) Transwell assay and quantitative analysis of Migratory cell ($n$ = 3). (J) Immunofluorescent staining of α-SMA and OPN in VSMCs ($n$ = 3). (K) Western blot and quantitative analysis of α-SMA and OPN in VSMCs ($n$ = 3). Data are expressed as mean ± SD (*$P$ < 0.05, **$P$ < 0.01 and ***$P$ < 0.005 were determined by one-way ANOVA and Tukey's *post hoc* test).

10 miRNAs collectively comprising over 60% of the total pool. Notably, miRNA164a/b-5p accounted for 51.47% of these top miRNAs.

Q-PCR further confirmed that miRNA-164a/b-5p and other enriched miRNAs were expressed in SL-ELNs (Fig. 4E). Notably, using default parameters (score threshold >140, energy threshold <−1 kcal $mol^{-1}$), the miRanda algorithm identified two potential binding sites between miRNA-164a/b-5p and the 3′ UTR of keap1. The first binding site had a score of 151 and an energy of −20.69 kcal $mol^{-1}$, while the second site had a score of 146 and an energy of −21.52 kcal $mol^{-1}$ (Fig. 4F and Fig. S5†).

Subsequently, dual luciferase reporter gene analysis was conducted to validate the regulatory effect of miRNA-164a/b-5p on Keap1. miRNA-164a/b-5p overexpression significantly attenuated the activity of the Keap1-3′UTR-wt reporter gene, whereas no discernible change was observed in the activity of the mutant reporter gene. Further, miRNA164a/b-5p mimics and inhibitors were synthesized and transfected into VSMCs. As illustrated in Fig. 4G, the exogenous administration of the miRNA164a/b-5p mimic induced a reduction in Keap1 expression. Notably, this effect was reversed upon the simultaneous addition of the inhibitor.

Finally, miRNA-164a/b-5p inhibitors were administered subsequent to SL-ELN treatment to further elucidate the role of miRNA-164a/b-5p in the effects mediated by SL-ELN. As depicted in Fig. 4H and I, both EDU staining and transwell assay results revealed a reversal in the SL-ELNs-induced attenuation of VSMC proliferation and migration upon inhibitor addition. Additionally, immunofluorescence and WB (Fig. 4J and K) analyses demonstrated that inhibitor administration mitigated the suppression of the VSMC phenotypic transition induced by SL-ELNs. These findings underscore the pivotal role of miRNA-164a/b-5p in mediating the inhibitory effects of SL-ELNs on phenotypic transition.

### miRNA164a/b-5p regulation of the Keap1/Nrf2 signaling pathway

Following the validation of the role of miRNA-164a/b-5p in SL-ELNs, its influence on the Keap1/Nrf2 signaling pathway was further examined. As a transcription factor, Nrf2 translocates from the cytoplasm to the nucleus in response to oxidative stress injury. This translocation initiates the transcription and translation of various antioxidant factors, thereby mitigating oxidative damage. Consequently, the expression of Nrf2 and downstream antioxidant factors was further assessed. Firstly, the WB results showed that SL-ELNs could inhibit the injury-induced increase in Keap1 expression and the decrease in Nrf2 expression in both *in vivo* and *in vitro* models (Fig. S6†). However, the introduction of the miRNA164a/b-5p inhibitor resulted in the restoration of Keap1 and Nrf2 expression. Therefore, miRNA164a/b-5p may contribute to the mitigation of vascular restenosis in SL-ELNs through the Keap1/Nrf2 pathway. Based on this, a mimic of miRNA164a/b-5p was used for further investigation. As depicted in Fig. 5A, PDGF-BB significantly downregulated the expression of Nrf2 as well as the antioxidant enzymes HO-1, catalase, and NQO1. Following the introduction of the miRNA 164a/b-5p mimic, these proteins exhibited a slight increase. However, this effect was reversed when Keap1 was overexpressed concurrently.

Furthermore, WB was utilized to distinguish between nuclear and cytoplasmic Nrf2 localization in VSMCs. PDGF-BB induced a decrease in nuclear Nrf2 protein levels while increasing cytoplasmic Nrf2 levels. Following the addition of the miRNA164a/b-5p mimic, Nrf2 expression increased in the nucleus and decreased in the cytoplasm. However, this effect was reversed following the overexpression of Keap1. Immunofluorescence (Fig. 5B) further corroborated these findings, revealing elevated nuclear Nrf2 expression in the presence of PDGF-BB and the miRNA164a/b-5p mimic, which was decreased upon Keap1 overexpression.

### miRNA164a/b-5p-mediated modulation of Keap1 to mitigate the phenotypic transition of VSMCs *in vitro* and *in vivo*

Finally, miRNA164a/b-5p was found to attenuate the phenotypic transition of VSMCs and improve restenosis after vascular injury by regulating Keap1. As illustrated in Fig. 5C, the transwell assay and EDU staining demonstrated that the miRNA164a/b-5p mimic significantly inhibited PDGF-BB-induced VSMC proliferation and migration. Furthermore, immunofluorescence (Fig. 5D) revealed that the miRNA164a/b-5p mimic effectively prevented VSMC phenotypic transformation. Additionally, to confirm whether the effect of miRNA164a/b-5p is Keap1-dependent, Keap1 overexpression was induced in VSMCs. Notably, these beneficial effects were abrogated by Keap1 overexpression.

Further validation was obtained using a mouse carotid artery injury model. Histological analysis *via* HE staining (Fig. 6A and B) revealed that treatment with the miRNA164a/b-5p mimic effectively mitigated injury-induced stenosis. However, this therapeutic effect was reversed following transfection with an AAV overexpressing Keap1. Immunofluorescence (Fig. 6C) analysis of vascular tissues indicated that the miRNA164a/b-5p mimic substantially reduced the injury-induced phenotypic transformation of VSMCs. Conversely, this effect was negated by Keap1 overexpression. Finally, WB (Fig. 6D) analysis demonstrated that the miRNA164a/b-5p mimic significantly attenuated the injury-induced phenotypic transformation, proliferation, and migration of VSMCs. However, Keap1 overexpression was observed to counteract these beneficial effects.

In summary, this study elucidated the role of miRNA164a/b-5p encapsulated in SL-ELNs in modulating VSMC behavior. Our findings indicate that miRNA164a/b-5p exerts its effects by downregulating Keap1 expression, thereby activating the Keap1/Nrf2 signaling pathway (Fig. 6E). This activation leads to a significant reduction in the phenotypic transition of VSMCs, ultimately mitigating vascular stenosis post-injury. These results underscore the potential therapeutic application of miRNA164a/b-5p in SL-ELN-based interventions for vascular pathologies.

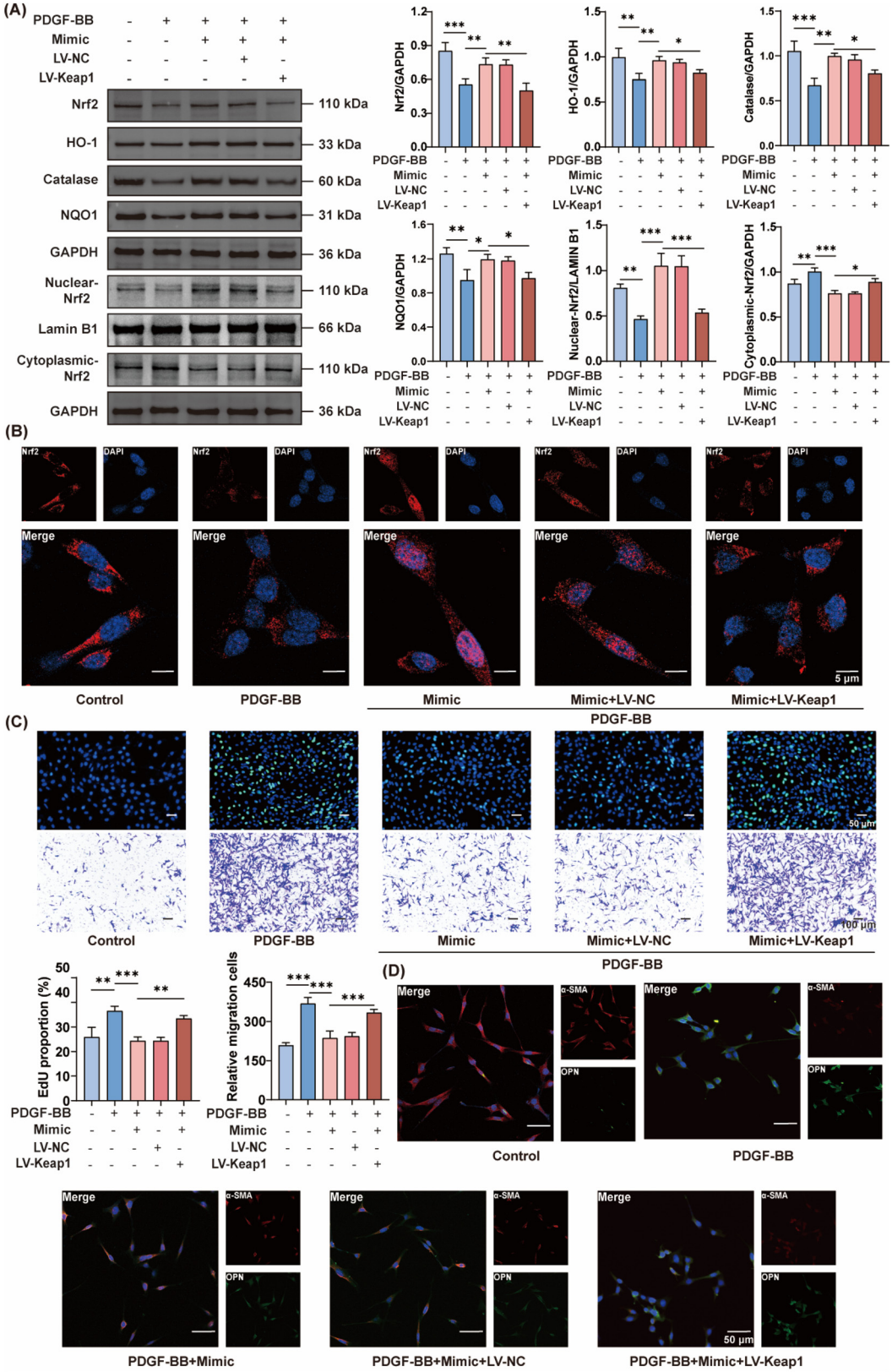


**Fig. 5** miRNA164a/b-5p regulation of the Keap1/Nrf2 signaling pathway and phenotypic transition of VSMCs *in vitro*. (A) Western blot and statistical analyses for protein level of Nrf2, HO-1, catalase, and NQO1 ($n$ = 3). (B) Immunofluorescent staining of Keap1 ($n$ = 3). (C) Image and quantitative analysis of EDU positive cell and transwell assay in VSMCs ($n$ = 3). (D) Immunofluorescent staining of α-SMA and OPN in VSMCs ($n$ = 3). Data are expressed as mean ± SD (*$P$ < 0.05, **$P$ < 0.01 and ***$P$ < 0.005 were determined by one-way ANOVA and Tukey's *post hoc* test).

## Discussion

Despite significant advancements in experimental and clinical studies, approximately 10–20% of interventional reconstructions for the restoration of atherosclerotic vascular circulation still fail owing to restenosis.[24] Currently, the only effective treatment for restenosis is repeat surgical intervention. Interventional procedures and mechanical dilatation cause damage or the detachment of vascular endothelial cells, triggering platelet adhesion and activation. This induces the release of multiple proinflammatory and growth factors, including PDGF and vascular endothelial growth factor (VEGF), and the generation of large amounts of ROS. Under pathological conditions, VSMCs undergo a phenotypic shift from a contractile to a synthetic phenotype, as indicated by a decrease in α-SMA and an increase in OPN.[25,26] This phenotypic shift prompts VSMCs to migrate towards the intima and undergo hyperproliferation, resulting in neointimal hyperplasia and ultimately leading to restenosis. Moreover, the remodeling of the extracellular matrix (ECM) is a crucial component in the restenosis processs.[27] Matrix metalloproteinases (MMPs), along with other protein hydrolases synthesized and released by VSMCs and macrophages, facilitate ECM breakdown, further promoting VSMC migration and proliferation.[28]

As a kind of extracellular vesicles with a diameter of 40–160 nm secreted by cells, exosomes could carry nucleic acids, proteins, lipids and other biologically active substances, which play an important role in normal physiological processes and disease development.[29] Previously, exosome research has predominantly focused on those derived from animals. However, in the past decade, PELNs have gradually attracted increasing attention from researchers.[30] Because this research is still in its nascent stages, specific markers for PELNs have not yet been identified. PELNs exhibit several advantages over animal exosomes, including broader availability, ease of large-scale production, lower extraction costs, superior biocompatibility, and reduced side effects[31] Consequently, PELNs are increasingly regarded as promising therapeutic agents or drug delivery systems for treating inflammation, infections, and autoimmune diseases. For example, ginger-derived ELNs have demonstrated potential for targeting the SARS-CoV-2 genome, presenting a novel therapeutic avenue.[32] Similarly, ELNs isolated from *Rhodiola rosea* reduce the expression of fibrosis marker genes and proteins in alveolar and mouse lung tissues.[33] Additionally, oat-derived ELNs exert anti-inflammatory effects, offering potential for preventing and treating brain inflammation-related diseases and enhancing memory function in alcohol-fed mice.[34] Notably, no PELNs have yet been reported for the treatment of restenosis following vascular injury. This present study isolated and purified SL-ELNs to explore their feasibility as potential therapeutic agents for inhibiting vascular restenosis. Different studies have utilized various purification bands as sources of PELNs, each containing bioactive components.[35] Considering that the purification bands within the 30–45% interval yielded higher quantities and the ELNs were more readily taken up by receptor cells, this interval was selected for this study, aligning with findings reported in most of the research.[36,37] In addition, it is worth noting that the therapeutic dose for mice in the present study was 1 mg $kg^{-1}$, which yielded a calculated human equivalent dose of 0.081 mg $kg^{-1}$. For a patient weighing 65 kg, this equates to approximately 5.27 mg of SL-ELNs (1.24 kg *Solanum lycopersicum*), which is impractical to achieve the therapeutic dose solely through diet. Therefore, purified SL-ELNs obtained *via* ultra-centrifugation are essential for meeting the required therapeutic standards.

Regardless of whether the exosomes are animal- or plant-derived, the bioactive components and their respective targeted genes and pathways have been a central focus of research. Numerous experiments have verified the phenomenon that plant miRNAs can cross-regulate physiological and pathological functions in mammals. Previous studies have demonstrated that vegetable-derived miR156 can target junctional adhesion molecule-A and reduce inflammatory cytokine-induced monocyte adhesion to vascular endothelial cells, thereby protecting blood vessels and ameliorating the progression of atherosclerosis.[38] Additionally, plant miRNA159 has been detected in human serum and has exhibited the potential to significantly inhibit the proliferation of breast cancer cells.[39] As effective natural carriers, miRNA-rich microvesicles can protect miRNAs from being degraded by nuclease, thereby enhancing their delivery in the animal body.[40] Based on this, miRNAs extracted from SL-ELNs were analyzed, revealing that miRNA164a/b-5p was highly expressed. As a widely expressed miRNA in *Solanum lycopersicum*, miR164 is encoded by four SIMIR164 genes, with miR164a and miR164b producing the same mature miRNA (miRNA164a/b-5p).[41] Dong *et al.* have found that miRNA-164a/b-5p can inhibit SINAM3 expression through an ethylene-dependent pathway, thereby enhancing the cold tolerance of *Solanum lycopersicum.*[42] However, the potential for cross-species regulatory effects from this miRNA remains unstudied. Our study demonstrated that miRNA164a/b-5p can target and suppress Keap1 expression, thereby activating the Keap1/Nrf2 signaling pathway and alleviating oxidative stress following vascular injury. As a critical component of the antioxidant pathway, Nrf2 is localized in the cytoplasm, where it binds with Keap1, undergoing ubiquitination and rapid degradation *via* the proteasome. Hence, inhibiting Keap1 expression significantly mitigates Nrf2 degradation, thereby facilitating its nuclear translocation and the subsequent activation of antioxidant gene expression. During vascular injury, these antioxidant responses are vital for maintaining redox homeostasis, effectively suppressing ROS levels, and ultimately attenuating the proliferation, migration, and phenotypic alteration of smooth muscle cells.

This study presents the successful synthesis of SL-ELNs and their preliminary effects on recurrence of vascular restenosis. However, further research is necessary to address existing limitations. The extraction of SL-ELNs is performed using the conventional method of differential ultracentrifugation combined with sucrose gradient centrifugation. This approach is

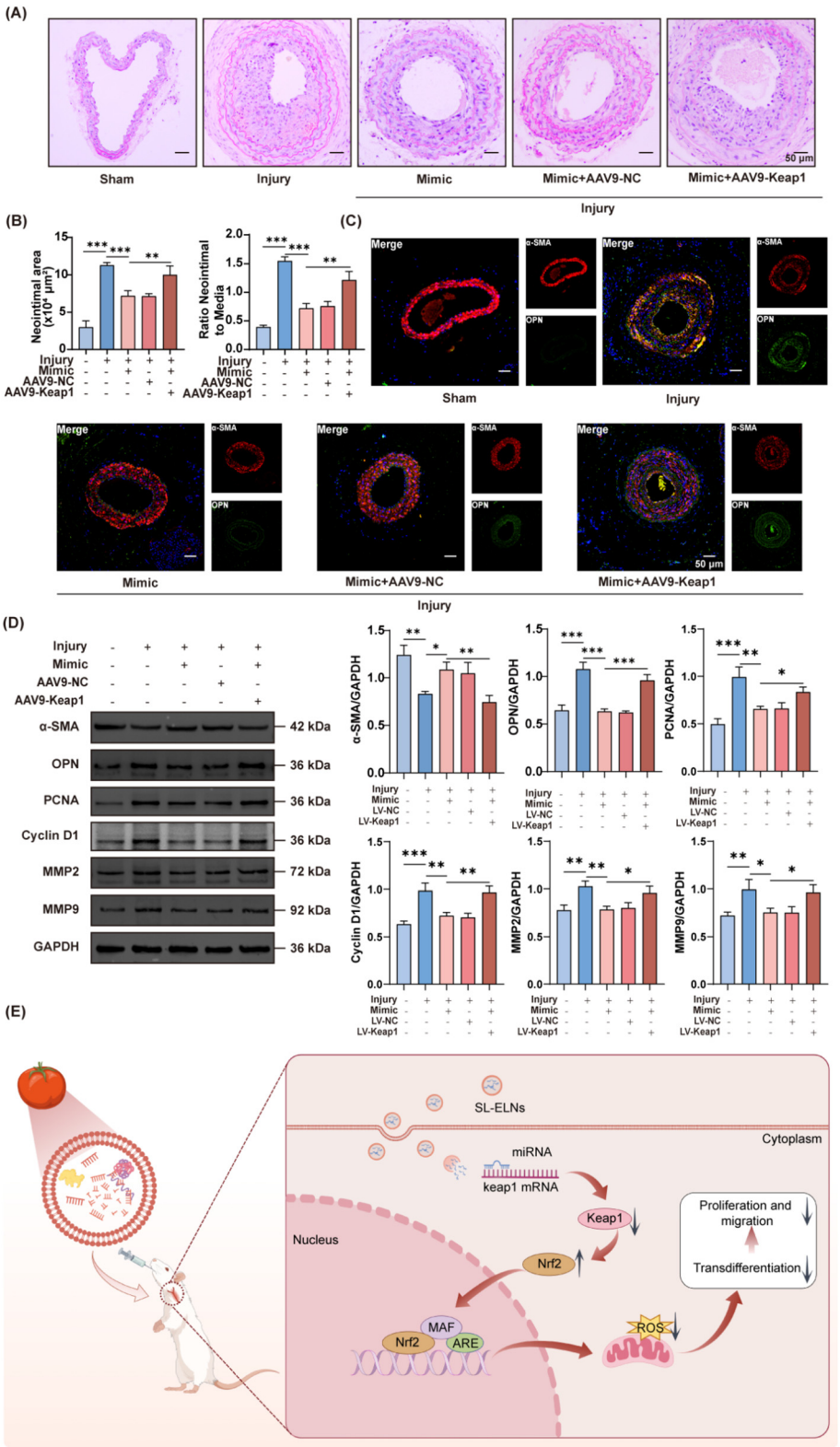


**Fig. 6** miRNA164a/b-5p-mediated modulation of Keap1 to mitigate the phenotypic transition of VSMCs *in vivo*. (A) HE staining image of carotid arteries in mice ($n$ = 3). (B) Statistical analyses for the neointima area and the ratio of neointima area to the media area in mouse carotid artery ($n$ = 3). (C) Immunofluorescent staining of α-SMA and OPN in mouse carotid artery ($n$ = 3). (D) Western blot and statistical analyses for protein level of α-SMA, OPN, PCNA, cyclin D1, MMP2 and MMP9 in mouse carotid artery ($n$ = 3). (E) Schematic of the mechanism by which SL-ELNs regulate vascular restenosis. Data are expressed as mean ± SD (*$P$ < 0.05, **$P$ < 0.01 and ***$P$ < 0.005 were determined by one-way ANOVA and Tukey's *post hoc* test).

complex and inefficient, necessitating the exploration of more straightforward and effective extraction techniques to enhance the yield and purity of the exosomes.[43] Moreover, our research focused exclusively on the role of miRNA within exosomes. Future studies should investigate the potential contributions of other bioactive substances (such as polyphenols and proteins) to the improvement of restenosis, thereby providing a comprehensive understanding of the therapeutic mechanisms of SL-ELNs.[44] Finally, exosome engineering has been shown to enhance therapeutic effects by inserting specific genes through transfection or gene editing.[45] The goal of future research is to apply engineered SL-ELNs in the treatment of vascular restenosis, thereby increasing their clinical application value.

## Conclusion

In this study, isolated and purified SL-ELNs exhibited potential for inhibiting vascular restenosis. The underlying mechanism involves miRNA164a/b-5p exerting an antioxidant effect by inhibiting Keap1 expression, thereby activating the Keap1/Nrf2 signaling pathway. In conclusion, the findings highlight the favorable biocompatibility and safety profile of SL-ELNs, suggesting their potential candidacy for preventing restenosis after vascular injury.

## Author contributions

Conception and design of manuscript: Hechen Shen, Dachang Liu and Meng Zhang; resources: Xiaomin Hu and Wenqing Gao; methodology: Hechen Shen, Yun Chang, and Xiaoyu Liang; drafted the manuscript: Hechen Shen and Meng Zhang; review and revision of manuscript: Xiaomin Hu and Wenqing Gao.

## Data availability

The data supporting this article have been included as part of the ESI.†

## Conflicts of interest

The authors declare that they have no competing interests.

## Acknowledgements

This work was sponsored by Key Project of Tianjin Natural Science Foundation (21JCZDJC00240), Tianjin Key Medical Discipline (Specialty) Construction Project (TJYXZDXK-035A), National Natural Science Foundation of China (82370420), Tianjin Health Research Project (TJWJ2022XK026, TJWJ2022MS020 and TJWJ2023XK018), Tianjin Science and Technology Project (21JCYBJC01250, 21JCYBJC01590 and 21JCQNJC01460) and Tianjin biomedical industry chain innovation Project (21ZXSYSY00030). We thank Bullet Edits Limited for the linguistic editing and proofreading of the manuscript.

## References

1 T. Koch, T. Lenz, T. Rheude, S. Cassese, M. Kazazi, E. Xhepa, T. Kessler, J. Wiebe, M. Ferenc, K. L. Laugwitz, M. Joner, H. Schunkert, A. Kastrati and S. Kufner, Recurrent Revascularization at 10 Years After Percutaneous Treatment of Drug-Eluting Stent Restenosis, *JACC Cardiovasc. Interv.*, 2024, **17**, 1–13.

2 K. Niu, C. Zhang, M. Yang, E. M. Maguire, Z. Shi, S. Sun, J. Wu, C. Liu, W. An, X. Wang, S. Gao, S. Ge and Q. Xiao, Small nucleolar RNA host gene 18 controls vascular smooth muscle cell contractile phenotype and neointimal hyperplasia, *Cardiovasc. Res.*, 2024, **120**, 796–810.

3 T. Melnik, O. Jordan, J. M. Corpataux, F. Delie and F. Saucy, Pharmacological prevention of intimal hyperplasia: A state-of-the-art review, *Pharmacol. Ther.*, 2022, **235**, 108157.

4 T. L. Kaeberlein, A. S. Green, G. Haddad, J. Hudson, A. Isman, A. Nyquist, B. S. Rosen, Y. Suh, S. Zalzala, X. Zhang, M. V. Blagosklonny, J. Y. An and M. Kaeberlein, Evaluation of off-label rapamycin use to promote healthspan in 333 adults, *Geroscience*, 2023, **45**, 2757–2768.

5 A. Kurdi, W. Martinet and G. R. Y. De Meyer, mTOR Inhibition and Cardiovascular Diseases: Dyslipidemia and Atherosclerosis, *Transplantation*, 2018, **102**, S44–S46.

6 N. P. Staff, J. C. Fehrenbacher, M. Caillaud, M. I. Damaj, R. A. Segal and S. Rieger, Pathogenesis of paclitaxel-induced peripheral neuropathy: A current review of in vitro and in vivo findings using rodent and human model systems, *Exp. Neurol.*, 2020, **324**, 113121.

7 L. Zhang, Y. Tao, R. Yang, Q. Hu, J. Jia, M. Yu, B. He, Z. Shen, H. Qin, Z. Yu and P. Chen, Euonymine inhibits in-stent restenosis through enhancing contractile phenotype of vascular smooth muscle cells via modulating the PTEN/AKT/mTOR signaling pathway, *Phytomedicine*, 2022, **107**, 154450.

8 A. Li, D. Li, Y. Gu, R. Liu, X. Tang, Y. Zhao, F. Qi, J. Wei and J. Liu, Plant-derived nanovesicles: Further exploration of biomedical function and application potential, *Acta Pharm. Sin. B.*, 2023, **13**, 3300–3320.

9 M. Trentini, I. Zanolla, E. Tiengo, F. Zanotti, E. Sommella, F. Merciai, P. Campiglia, D. Licastro, M. Degasperi, L. Lovatti, M. Bonora, A. Danese, P. Pinton and B. Zavan, Link between organic nanovescicles from vegetable kingdom and human cell physiology: intracellular calcium signalling, *J. Nanobiotechnol.*, 2024, **22**, 68.

10 J. H. Hwang, Y. S. Park, H. S. Kim, D. H. Kim, S. H. Lee, C. H. Lee, S. H. Lee, J. E. Kim, S. Lee, H. M. Kim, H. W. Kim, J. Kim, W. Seo, H. J. Kwon, B. J. Song, D. K. Kim, M. C. Baek and Y. E. Cho, Yam-derived

exosome-like nanovesicles stimulate osteoblast formation and prevent osteoporosis in mice, *J. Controlled Release*, 2023, **355**, 184–198.

11 J. Liu, J. Xiang, C. Jin, L. Ye, L. Wang, Y. Gao, N. Lv, J. Zhang, F. You, H. Qiao and L. Shi, Medicinal plant-derived mtDNA via nanovesicles induces the cGAS-STING pathway to remold tumor-associated macrophages for tumor regression, *J. Nanobiotechnol.*, 2023, **21**, 78.

12 N. Gürbüz Çolak, N. T. Eken, M. Ulger, A. Frary and S. Doganlar, Mapping of quantitative trait loci for antioxidant molecules in tomato fruit: Carotenoids, vitamins C and E, glutathione and phenolic acids, *Plant Sci.*, 2020, **292**, 110393.

13 N. Li, X. Wu, W. Zhuang, L. Xia, Y. Chen, C. Wu, Z. Rao, L. Du, R. Zhao, M. Yi, Q. Wan and Y. Zhou, Tomato and lycopene and multiple health outcomes: Umbrella review, *Food Chem.*, 2021, **343**, 128396.

14 M. Mazidi, G. A. Ferns and M. Banach, A high consumption of tomato and lycopene is associated with a lower risk of cancer mortality: results from a multi-ethnic cohort, *Public Health Nutr.*, 2020, **23**, 1569–1575.

15 D. Murcia-Lesmes, I. Dominguez-Lopez, E. P. Laveriano-Santos, A. Tresserra-Rimbau, S. Castro-Barquero, R. Estruch, Z. Vazquez-Ruiz, M. Ruiz-Canela, C. Razquin, D. Corella, J. V. Sorli, J. Salas-Salvado, K. A. Perez-Vega, E. Gomez-Gracia, J. Lapetra, F. Aros, M. Fiol, L. Serra-Majem, X. Pinto, E. Ros and R. M. Lamuela-Raventos, Association between tomato consumption and blood pressure in an older population at high cardiovascular risk: observational analysis of PREDIMED trial, *Eur. J. Prev. Cardiol.*, 2024, **31**, 922–934.

16 L. Hu, Q. Liu, Y. Ou, D. Li, Y. Wu, H. Li, Z. Zhu and M. Liang, Dietary lycopene is negatively associated with abdominal aortic calcification in US adults: a cross-sectional study, *Ann. Med.*, 2023, **55**, 2195205.

17 S. Przybylska and G. Tokarczyk, Lycopene in the Prevention of Cardiovascular Diseases, *Int. J. Mol. Sci.*, 2022, **23**, 1957.

18 Y. Jia, C. Mao, Z. Ma, J. Huang, W. Li, X. Ma, S. Zhang, M. Li, F. Yu, Y. Sun, J. Chen, J. Feng, Y. Zhou, Q. Xu, L. Zhao, Y. Fu and W. Kong, PHB2 Maintains the Contractile Phenotype of VSMCs by Counteracting PKM2 Splicing, *Circ. Res.*, 2022, **131**, 807–824.

19 E. Berger, P. Colosetti, A. Jalabert, E. Meugnier, O. P. B. Wiklander, J. Jouhet, E. Errazurig-Cerda, S. Chanon, D. Gupta, G. J. P. Rautureau, A. Geloen, S. El-Andaloussi, B. Panthu, J. Rieusset and S. Rome, Use of Nanovesicles from Orange Juice to Reverse Diet-Induced Gut Modifications in Diet-Induced Obese Mice, *Mol. Ther.–Methods Clin. Dev.*, 2020, **18**, 880–892.

20 Y. Mao, M. Han, C. Chen, X. Wang, J. Han, Y. Gao and S. Wang, A biomimetic nanocomposite made of a ginger-derived exosome and an inorganic framework for high-performance delivery of oral antibodies, *Nanoscale*, 2021, **13**, 20157–20169.

21 C. Ouyang, J. Li, X. Zheng, J. Mu, G. Torres, Q. Wang, M. H. Zou and Z. Xie, Deletion of Ulk1 inhibits neointima formation by enhancing KAT2A/GCN5-mediated acetylation of TUBA/alpha-tubulin in vivo, *Autophagy*, 2021, **17**, 4305–4322.

22 F. Long, D. Yang, J. Wang, Q. Wang, T. Ni, G. Wei, Y. Zhu and X. Liu, SMYD3-PARP16 axis accelerates unfolded protein response and mediates neointima formation, *Acta Pharm. Sin. B*, 2021, **11**, 1261–1273.

23 R. Garcia-Martin, G. Wang, B. B. Brandao, T. M. Zanotto, S. Shah, S. Kumar Patel, B. Schilling and C. R. Kahn, MicroRNA sequence codes for small extracellular vesicle release and cellular retention, *Nature*, 2022, **601**, 446–451.

24 C. Huang, J. Zhao and Y. Zhu, Drug-Eluting Stent Targeting Sp-1-Attenuated Restenosis by Engaging YAP-Mediated Vascular Smooth Muscle Cell Phenotypic Modulation, *J. Am. Heart Assoc.*, 2020, **9**, e014103.

25 M. Wu, M. Xun and Y. Chen, Adaptation of Vascular Smooth Muscle Cell to Degradable Metal Stent Implantation, *ACS Biomater. Sci. Eng.*, 2023, **9**, 4086–4100.

26 J. W. Jukema, J. J. Verschuren, T. A. Ahmed and P. H. Quax, Restenosis after PCI. Part 1: pathophysiology and risk factors, *Nat. Rev. Cardiol.*, 2011, **9**, 53–62.

27 X. Chen, J. Xu, W. Bao, H. Li, W. Wu, J. Liu, J. Pi, B. Tomlinson, P. Chan, C. Ruan, Q. Zhang, L. Zhang, H. Fan, E. Morrisey, Z. Liu, Y. Zhang, L. Lin, J. Liu and T. Zhuang, Endothelial Foxp1 Regulates Neointimal Hyperplasia Via Matrix Metalloproteinase-9/Cyclin Dependent Kinase Inhibitor 1B Signal Pathway, *J. Am. Heart Assoc.*, 2022, **11**, e026378.

28 J. Shen, J. B. Song, J. Fan, Z. Zhang, Z. J. Yi, S. Bai, X. L. Mu, Y. B. Yang and L. Xiao, Distribution and Dynamic Changes in Matrix Metalloproteinase (MMP)-2, MMP-9, and Collagen in an In Stent Restenosis Process, *Eur. J. Vasc. Endovasc. Surg.*, 2021, **61**, 648–655.

29 R. Kalluri and V. S. LeBleu, The biology, function, and biomedical applications of exosomes, *Science*, 2020, **367**, eaau6977.

30 M. Cao, N. Diao, X. Cai, X. Chen, Y. Xiao, C. Guo, D. Chen and X. Zhang, Plant exosome nanovesicles (PENs): green delivery platforms, *Mater. Horiz.*, 2023, **10**, 3879–3894.

31 H. A. Dad, T. W. Gu, A. Q. Zhu, L. Q. Huang and L. H. Peng, Plant Exosome-like Nanovesicles: Emerging Therapeutics and Drug Delivery Nanoplatforms, *Mol. Ther.*, 2021, **29**, 13–31.

32 S. P. Kalarikkal and G. M. Sundaram, Edible plant-derived exosomal microRNAs: Exploiting a cross-kingdom regulatory mechanism for targeting SARS-CoV-2, *Toxicol. Appl. Pharmacol.*, 2021, **414**, 115425.

33 J. Du, Z. Liang, J. Xu, Y. Zhao, X. Li, Y. Zhang, D. Zhao, R. Chen, Y. Liu, T. Joshi, J. Chang, Z. Wang, Y. Zhang, J. Zhu, Q. Liu, D. Xu and C. Jiang, Plant-derived phosphocholine facilitates cellular uptake of anti-pulmonary fibrotic HJT-sRNA-m7, *Sci. China: Life Sci.*, 2019, **62**, 309–320.

34 F. Xu, J. Mu, Y. Teng, X. Zhang, K. Sundaram, M. K. Sriwastva, A. Kumar, C. Lei, L. Zhang, Q. M. Liu, J. Yan, C. J. McClain, M. L. Merchant and H. G. Zhang, Restoring Oat Nanoparticles Mediated Brain Memory Function of Mice Fed Alcohol by Sorting Inflammatory

 

Dectin-1 Complex Into Microglial Exosomes, *Small*, 2022, **18**, e2105385.

35 M. Zu, D. Xie, B. S. B. Canup, N. Chen, Y. Wang, R. Sun, Z. Zhang, Y. Fu, F. Dai and B. Xiao, 'Green' nanotherapeutics from tea leaves for orally targeted prevention and alleviation of colon diseases, *Biomaterials*, 2021, **279**, 121178.

36 C. Gao, Y. Zhou, Z. Chen, H. Li, Y. Xiao, W. Hao, Y. Zhu, C. T. Vong, M. A. Farag, Y. Wang and S. Wang, Turmeric-derived nanovesicles as novel nanobiologics for targeted therapy of ulcerative colitis, *Theranostics*, 2022, **12**, 5596–5614.

37 H. Cai, L. Y. Huang, R. Hong, J. X. Song, X. J. Guo, W. Zhou, Z. L. Hu, W. Wang, Y. L. Wang, J. G. Shen and S. H. Qi, Momordica charantia Exosome-Like Nanoparticles Exert Neuroprotective Effects Against Ischemic Brain Injury via Inhibiting Matrix Metalloproteinase 9 and Activating the AKT/GSK3beta Signaling Pathway, *Front. Pharmacol.*, 2022, **13**, 908830.

38 D. Hou, F. He, L. Ma, M. Cao, Z. Zhou, Z. Wei, Y. Xue, X. Sang, H. Chong, C. Tian, S. Zheng, J. Li, K. Zen, X. Chen, Z. Hong, C. Y. Zhang and X. Jiang, The potential atheroprotective role of plant MIR156a as a repressor of monocyte recruitment on inflamed human endothelial cells, *J. Nutr. Biochem.*, 2018, **57**, 197–205.

39 A. R. Chin, M. Y. Fong, G. Somlo, J. Wu, P. Swiderski, X. Wu and S. E. Wang, Cross-kingdom inhibition of breast cancer growth by plant miR159, *Cell Res.*, 2016, **26**, 217–228.

40 M. Muskan, P. Abeysinghe, R. Cecchin, H. Branscome, K. V. Morris and F. Kashanchi, Therapeutic potential of RNA-enriched extracellular vesicles: The next generation in RNA delivery via biogenic nanoparticles, *Mol. Ther.*, 2024, **32**, 2939–2949.

41 S. K. Gupta, A. Vishwakarma, H. D. Kenea, O. Galsurker, H. Cohen, A. Aharoni and T. Arazi, CRISPR/Cas9 mutants of tomato MICRORNA164 genes uncover their functional specialization in development, *Plant Physiol.*, 2021, **187**, 1636–1652.

42 Y. Dong, M. Tang, Z. Huang, J. Song, J. Xu, G. J. Ahammed, J. Yu and Y. Zhou, The miR164a-NAM3 module confers cold tolerance by inducing ethylene production in tomato, *Plant J.*, 2022, **111**, 440–456.

43 S. Suharta, A. Barlian, A. C. Hidajah, H. B. Notobroto, I. D. Ana, S. Indariani, T. D. K. Wungu and C. H. Wijaya, Plant-derived exosome-like nanoparticles: A concise review on its extraction methods, content, bioactivities, and potential as functional food ingredient, *J. Food Sci.*, 2021, **86**, 2838–2850.

44 C. X. Wu and Z. F. Liu, Proteomic Profiling of Sweat Exosome Suggests its Involvement in Skin Immunity, *J. Invest. Dermatol.*, 2018, **138**, 89–97.

45 J. Mondal, S. Pillarisetti, V. Junnuthula, M. Saha, S. R. Hwang, I. K. Park and Y. K. Lee, Hybrid exosomes, exosome-like nanovesicles and engineered exosomes for therapeutic applications, *J. Controlled Release*, 2023, **353**, 1127–1149.